Progress in Physics of Applied Materials 7 (2027), Serial Number 14, 9-15

Semnan University

Progress in Physics of Applied Materials

journal homepage: https://ppam.semnan.ac.ir/

Characterization of Tungsten Carbide and Bismuth Tungstate Nanostructured Composites for High-Energy Photon Attenuation

Haneen Jabaar Hawi, Mustafa Shakir Hashim *

Physics department, Education College, Mustansiriyah University, Baghdad-Iraq

ARTICLE INFO

Article history:
Received: 11 May 2026
Revised: 24 May 2026
Accepted: 31 May 2026
Published online: 13 June 2026

Keywords:
Gamma shielding;
Bismuth Tungstate;
Nanoparticles.

ABSTRACT

The novelty and significance of the multilayer shielding design is introduced in current paper. Two dense nontoxic powders were utilized to fabricate gamma attenuation shielding. Tungsten carbide (WC) and bismuth tungstate were deposited on 316L SS discs separately by electrophoretic and dip coating techniques. Four samples were synthesized. The first sample consists of ten coated discs with WC and fixed by epoxy. The second sample is like the first one, but the coating material is bismuth tungstate. The third and fourth samples were a mixture of epoxy, 316L SS micropowder plus WC, and bismuth tungstate, respectively. The hydrothermal technique was used to prepare bismuth tungstate. Bismuth tungstate powder was characterized using the X-ray diffraction (XRD) technique. Scanning electron microscope (SEM) images showed that the average particle size of bismuth tungstate was about 60 nm. Shielding properties like linear absorption coefficient (LAC), transmission factor percentage (T%), and radiation protection efficiency (RPE%) were calculated for all samples. The coating of 316L SS plates with WC and bismuth tungstate nanoparticles increases LAC. The incorporation of these nanoparticles and micro 316L SS into the epoxy matrix significantly enhanced the composites' ability to attenuate gamma radiation, as demonstrated by the increased LAC. The result confirms the importance of having high atomic numbers with high density of materials that make up shield, and the presence of voids in these materials will greatly weaken them even if the atomic numbers are high.

1. Introduction

As nuclear technology advances and its widespread use in modern industries increases, more people are likely to be exposed to ionizing radiation. Shielding is essential to absorb and reduce radiation intensity.

Producing homogeneous composite mixtures of component materials is challenging, especially if different wt% of particles of different sizes, shapes, and weights are included in a polymer matrix, as it takes time for the composite to solidify and some heavy particles may settle at the bottom. This problem can be solved by applying a multi-layer shielding approach [1].

To provide adequate protection from a wide range of ionizing radiation types, multi-layer shielding often requires the use of a combination of materials, each with its own unique properties. The materials used vary depending on the application, and the thickness of each layer is also an important factor. Multiple layers of radiation shielding can provide better protection from ionizing radiation. This is achieved by increasing the amount of material through which photons must pass, which in turn reduces their intensity. This strategy has the potential to provide additional protection from scattered radiation, as well as from secondary radiation resulting from radiation transmission through the shields [2].

* Corresponding author.
E-mail address: mustmust@uomustansiriyah.edu.iq

Cite this article as:

Hawi. H.J. and Hashim, M.S., 2027. Characterization of Tungsten Carbide and Bismuth Tungstate Nanostructured Composites for High-Energy Photon Attenuation. *Progress in Physics of Applied Materials*, *7*(1), pp.9-15. DOI: 10.22075/ppam.2026.41152.1226

Rather than sticking with the radiation protection capability of a single layer, many researchers have begun to evaluate dual-layer and multi-layer shields, with some of these experimental combinations yielding good attenuation properties and potentially being considered alternatives to lead [3]. The two types of shielding configurations are composites and mixtures. Additives are mixed with a base material to enhance the material capacity to shield. Since composite solidification takes time and some heavy particles may settle to the bottom, it can be difficult to produce homogeneous composite mixes from the component materials. The application of a multilayer shielding method can help avoid those issues [4,5].

The radiation shielding properties of tungsten based materials were investigated by many researchers. Because of its non-toxic qualities and excellent efficacy in attenuating neutron radiation, Chang et al. demonstrated that tungsten is a potential material to replace traditional lead [6].

High atomic packing, a large heat absorption cross-section, a big macroscopic slowing down power atoms, and a large attenuation coefficient for high-energy gamma contribution are among the advantageous nuclear features of tungsten carbide (WC). It also possesses outstanding industrial and thermophysical qualities [7]. A research by Soylu et al. demonstrated that at 364 keV and 662 keV gamma photon energies, the radiation shielding effectiveness of a composite made of WC and ethylene vinylacetate was comparable to that of lead [8]. Giménez et al. have optimized the radiation shielding design for small and medium reactors by using lead as a filler material with sintered tungsten carbide pellets [9].

Bismuth tungstate is a popular substance with several uses in electronic component manufacturing. This flexible material may be utilized for many applications such as capacitors, humidity detectors, optical sensors, and thermistors [10]. Bi_2WO_6 has two high Z elements, non-toxic and environmentally benign elements, tungsten (W) and Bi, making it an ideal alternative for Pb in radiation shielding materials [11]. Bi_2WO_6 has a classic Aurivillius oxide structure with layered perovskites and has been widely used in photocatalytic degradation. However, research on its applicability in radiation protection is restricted [12].

Mixing 316L SS with WC (or bismuth tungstate) and epoxy creates a triple-action protective shield. The radiation shielding efficacy of the proposed composite relies on a synergistic, triple-action mechanism where the physical properties of each constituent target specific radiation types and energy range. Specifically, the tungsten carbide/bismuth tungstate nanoparticles utilize tungsten's high atomic number (Z) to maximize low to medium energy gamma-ray absorption via the photoelectric effect. This mechanism directly complements the 316L SS matrix, whose moderate density and intermediate atomic number effectively attenuate higher-energy gamma photons through Compton scattering, progressively reducing their energy. Concurrently, the hydrogen-rich epoxy matrix serves as a low Z neutron moderator, slowing down fast neutrons through elastic scattering to facilitate their ultimate capture. Together, these three components form an integrated shield that simultaneously mitigates a mixed neutron-gamma radiation spectrum across a wide energy range.

The purposes of this contribution are to investigate (i) the shielding properties of multilayer materials that were made from coated 316L SS with WC and bismuth tungstate, respectively and, (ii) the shielding properties of mixtures made from micro 316L SS, epoxy, and WC (or Bi2WO6) nanoparticles.

2. Experimental procedures and details

Tungsten Carbide (WC) nanopowder was purchased from US Research Nanomaterials, Inc. According to this company, the WC powder has a hexagonal structure with a size ≈ of approximately 50 nm.

Bismuth tungstate was prepared by the hydrothermal technique. The procedure is as follows: Solution A was prepared by dissolving $Bi(NO_3)_3.5H_2O$ (1.8 g) in diluted nitric acid (1 ml (HNO_3) : 15 ml (distilled water)). Solution B was set by dissolving Na_2WO_6 (0.453 g) in distilled water (80 ml). By dropping solution A on solution B slowly with stirring, the two solutions were mixed, and the formed solution became clear. The produced solution was put in an autoclave, and then the heat (200°C) was applied to it for 20 hours. After the hydrothermal process, the autoclave was left to cool to room temperature. The solution was washed with water and ethanol three times. The formed powder (bismuth tungstate) was characterized by X-ray diffraction (XRD); (model Shimadzu-japan) and scanning electron microscope (SEM); (model TESCAN MIRA3-Frech) techniques.

Ten 316L SS discs were coated with WC nanoparticles using the electrophoretic deposition technique. Inside a simple electric cell, two 316L SS discs were utilized as cathode and anode (the distance between them is 0.5 cm). The applied voltage between two discs was 250V with direct current of 100mA. Due to a very thin layer of coating, the thickness was increased by the dip coating method. After immersing the 316L SS discs inside the suspension of WC in ethanol solution, the thickness of both sides was increased.

The same coating process was repeated to deposit bismuth tungstate on ten 316L SS discs. The coated discs were arranged and put on each other and then fixed with epoxy.

For multilayer samples, the total thickness of epoxy layers, ten 316L discs, and WC powder layers are 4.7, 10, and 1.6 mm, respectively. Approximately, the same layers' thicknesses were for bismuth tungstate. Archimedes' method was used to calculate Bulk density and true density.

A gamma ray spectroscopy system with a NaI(Tl) detector was utilized to measure gamma attenuation properties of the fabricated samples. The detector consists of a single crystal of thallium-activated sodium iodide optically coupled to the photocathode of a photomultiplier tube. Am^{241}, Ca^{137}, and Co^{60} were used as a source of gamma ray. The distance between the sources and detector was 10cm. For each measurement, the spectrum was stripped of background. UCS-30 software was utilized to record the spectrum. Also, this software gives the ability to spate the net counts from cross counts.

3. Results and Discussion

XRD pattern of the synthesized bismuth tungstate is illustrated in Figure 1. The characteristic peaks observed in this figure correspond to the orthorhombic Russellite structure (PDF# 26-1044) alongside a secondary cubic bismuth tungsten oxide phase ($Bi_{3.84}W_{0.16}O_{6.24}$, PDF# 43-0447).

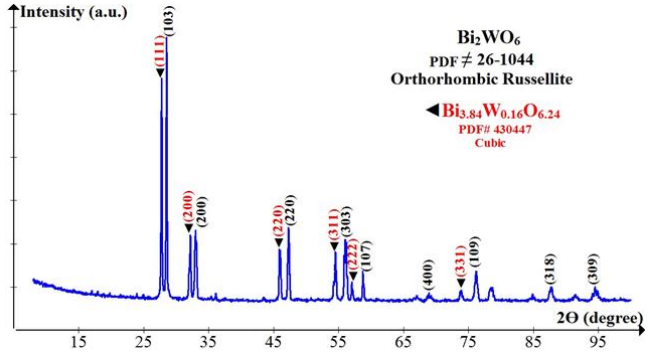

Fig. 1. XRD of Bi_2WO_6 nanoparticles.

There are two phases formed for synthesized bismuth tungstate: orthorhombic and cubic, matched to PDF# 26-1044 and PDF# 430447, respectively. Ten peaks can be recorded for the major phase (orthorhombic): (103), (200), (220), (303), (107), (400), (109), (307), (318), and (309). There are six peaks for the second phase (cubic): (111), (200), (220), (311), (222), and (331). The formation of the cubic phase may be due to one or all of the following reasons: a non-stoichiometric, oxygen-deficient, incomplete crystallization, and partial transformation during synthesis [13]. The presence of the cubic $Bi_{3.84}W_{0.16}O_{6.24}$ phase shows a competitive kinetic pathway during hydrothermal process, causing an incomplete phase transformation to pure orthorhombic Bi_2WO_6. Under the chosen synthesis conditions, this cubic phase acts as a stable secondary phase rather than an amorphous, poorly crystallized impurity, as evidenced by its well-defined, sharp diffraction peaks (e.g., at (111), (200), and (220)). From a radiation shielding viewpoint, the dense, bismuth-rich nature of this cubic phase guarantees that the total linear and mass attenuation cross-sections remain highly effective for gamma-ray interaction.

The morphology of the synthesized bismuth tungstate is shown in Figure 2. The clusters formed vary in size and shape, with the size of a single cluster extending from nanometers to several micrometers. Aggregation, or clustering, which is typical in the hydrothermal technique, is clear in the images. The use of high temperatures in this technique can influence the crystal structure, leading to particle accumulation and the construction of larger crystals [14]. From Figure 2, one can observe a highly crystalline, irregular plate-like and nanoscale grain morphology. The sharp edges and defined facets suggest a well-crystallized product, consistent with XRD results.

The density of the shielding material and its porosity are other important parameters that affect its performance in attenuation of gamma rays. The calculation results of these parameters were tabulated in table 1.

The porosity percentage is greater for bismuth tungstate compared with that for WC. According to porosity values, voids exist in all powders. The presence of gaps negatively affects the properties of the shielding element and hinders the improvement of radiation protection effectiveness [15].

To calculate the experimental linear absorption coefficient (LAC) for tungsten carbide powders, the intensity of a transmitted gamma ray through the discs of the powders is measured. It is clear from Figure 3 that the intensity is reduced with increasing the thickness of WC powder.

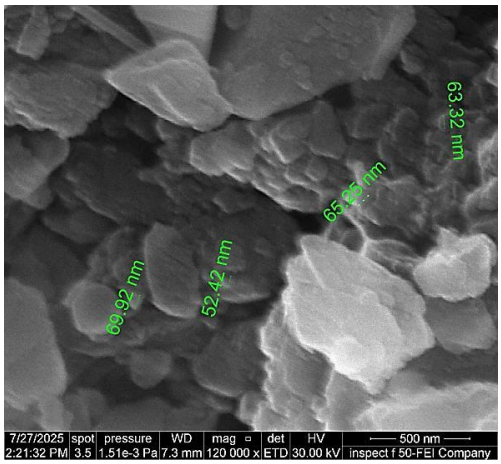

Fig. 2. FE-SEM image of the synthesized Bi_2WO_6 nanoparticles. The individual nanoparticle dimensions are highlighted by the green measurement annotations, indicating an average grain size distributed in the range of approximately 52 nm to 70nm.

Furthermore, with increasing the energy, the Gamma-ray spectra come closer to each other. The behavior of curves in Figure 3 represents Beer-Lambert's law, which illustrates the exponential relationship between the intensity of incident radiation and the intensity of transmitted radiation through an absorbing medium. This result is in agreement with that in [16].

Using this law, LACs were calculated for WC powder as shown in Figure 4. With increasing energy, LAC values decrease due to the increase in gamma ability to penetrate the powder. As energy increases, LAC decreases sharply and flattens after ~1 MeV. Experimental results match well with theoretical predictions (using the XCOM database), with small deviations likely due to density (the powder contains voids, so effective density is slightly lower, and scattering and absorption differ). Also, experimental conditions include secondary effects (scattering from surroundings, detector efficiency, and backscattered photons), leading to deviations.

It is important to remember that the XCOM database (Photon Cross Sections Database developed by NIST (National Institute of Standards and Technology) does not contain information on solid-state or molecular effects. Only isolated, independent neutral atoms are listed in the elemental cross-sections. Therefore, differences may arise

between experimental results and XCOM results in complex composite [17].

Gaps were found between the dots in LAC experimental curve, see Figure 4, as a result of using only four radioactive sources, which may indicate one of the possible interactions between the incoming photons and the powder. For example, see the inset of Figure 4, the photoelectric absorption of WC occurs at an energy of ≈ 0.07 MeV, an energy that is not observable. To address these issues, researchers may utilize purely theoretical methods to compute the shielding properties, such as the MONTE CARLO simulation, for instance [18].

The same procedure was repeated to calculate LAC for bismuth tungstate. Again, there is a reduction in the intensity of spectra, but compared with that of WC, it is less, referring to the superiority of WC nanoparticles.

Because Compton scattering is dominant at higher photon energies and photoelectric effect is dominant at lower photon energies, this trend is common. Actual uncertainties (thickness, detector efficiency, and counting error) may cause slight differences between actual results and theoretical predictions. Minor variations in the composition or density of the bismuth tungstate sample may also occur. The validity of the experimental approach and the protective potential of bismuth tungstate were confirmed by the good agreement between the experimental and theoretical results.

Table 1. Some structural properties for the used powders.

The powder	Bulk density [g /cm^3]	True density [g /cm^3]	Porosity%
Tungsten Carbide	4.3	9.919	31.31
Bismuth Tungstate	3.05	6.397	47.8

The attenuation for (WC powder + epoxy), (WC powder + epoxy+ 316LSS powder), and (WC powder + epoxy + 316L SS plates) are drown in Figure 5. Especially in the Compton range (200–650 keV) and at the full power peak (around 660 keV), plus other peaks above 1 MeV), the WC three shields reduce the count rate. This result is in agreement with that in. Gamma spectra as a function of energy for bismuth tungstate as a shield are also shown in Figure 5. Again, the synthesized samples attenuate gamma rays; the degree of attenuation depends on the values of atomic numbers and the amount of voids inside each sample.

Analysis of the curves in Figure 5 and the data in Table 1 reveal that the WC+316L SS powder composite has superior performance compared to the bismuth tungstate +316L SS powder composite, due to its higher true density, and higher filling efficiency between the metal powder and the carbide filler. Adding 316L powder to a WC-epoxy matrix results in a much higher final density compared to adding it to a bismuth tungstate matrix.

To evaluate the WC and bismuth tungstate shielding efficiency, transmission% and RPE% were calculated and drown in Figure 6. At low energy, all samples have high RPE% and low transmission%. At moderate energies, the presence of plates inside the third sample is a crucial factor that enhances the reduction of gamma counts. This might be due to the minimization of voids that my existence with 316L SS powder. At high energy, gamma attenuation by all samples reduces to its minimum values due to the increasing of gamma ability to crossing the samples. This outcome is consistent with [19].

For bismuth tungstate, T% increases with increasing gamma energy, as observed in Figure 6. The photoelectric effect is dominant at low energy but at intermediate energies the Compton scattering becomes dominant. T% increases at high energies, referring to reduced RPE% as Figure 6 shows. The adding of 316L SS powder improves RPE% due to increasing effective density of epoxy which has low density and effective atomic number. However, the existence of voids between particles reduces the RPE%. RPE% increases with using 316L SS plates, as a result to continuous plate geometry which provides better photon interaction probability. Also, the photon leakage paths were reduced by these plates.

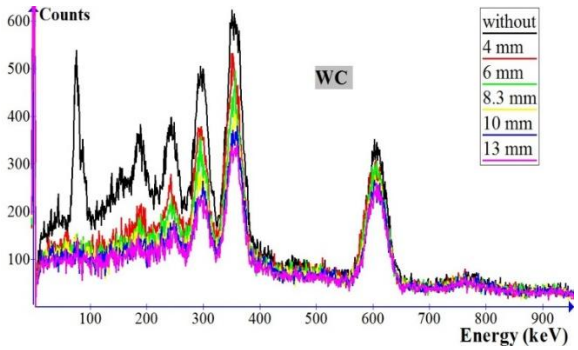

Fig. 3. Gamma-ray pulse height spectra (intensity in counts vs. photon energy in keV) transmitted through tungsten carbide (WC) powder of varying thicknesses.

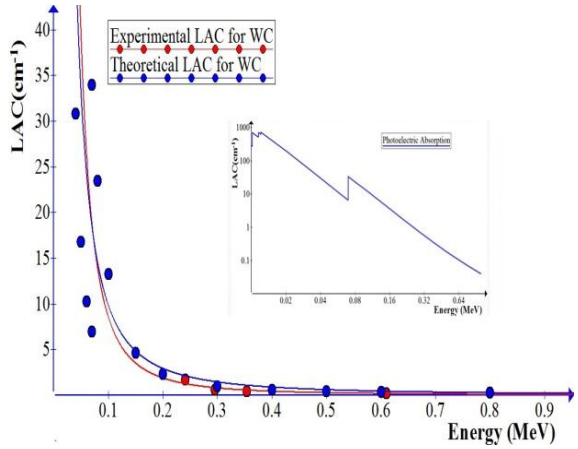

Fig. 4. Linear attenuation coefficient of the tungsten carbide powder as a function of incident gamma-ray energy (0 to 0.9 MeV). The plot provides a validation comparison between the experimental data points and the theoretical predictions. Inset shows the photoelectric absorption of WC occured at an energy of ≈ 0.07 MeV.

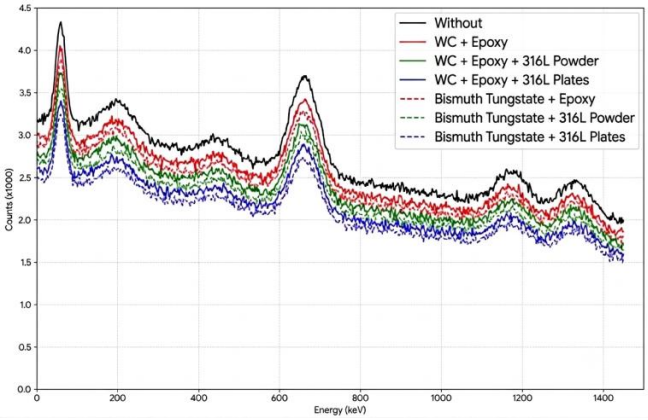

Fig. 5. Comparative gamma-ray pulse height transmission spectra vs. photon energy (comparing the shielding performance of multilayer WC and bismuth tungstate samples).

The behavior of LAC curves in Figure 7 appears similar, where attenuation increases at low energies due to the photoelectric effect, and as energy increases, the shielding against gamma rays decreases. In the mid-energy range, Compton scattering again becomes dominant, but at high energies, attenuation decreases significantly across the entire samples.

The effectiveness of radiation shielding depends heavily on the atomic number (Z), especially at low energy levels dominated by the photoelectric effect (which has a Z^{4-5} dependence). Although bismuth (Bi, Z=83) has a higher atomic number than tungsten (W, Z=74), the tungsten carbide (WC) system has a higher wt% of heavier atoms per unit volume. In bismuth tungstate (Bi_2WO_6), there are six light oxygen atoms for every tungsten atom and two bismuth atoms, which reduce the effective atomic number of the compound and thus the density of radiation-absorbing atoms.

The low porosity of the WC+SS system ensures a more continuous and less permeable physical barrier to radiation, thus enhancing its absorption capacity. Conversely, the low density of bismuth tungstate composite may result in relatively unshielded pathways within the material, allowing for higher "radiative flux" through regions dominated by the less dense resinous material (such as epoxy) in the composite.

The use of 316L SS plates represents a strategic shift in protection philosophy. Unlike powders mixed to improve the properties of the resin from within, these plates act as solid, independent physical barriers, blocking radiation through the principles of geometric insulation and density.

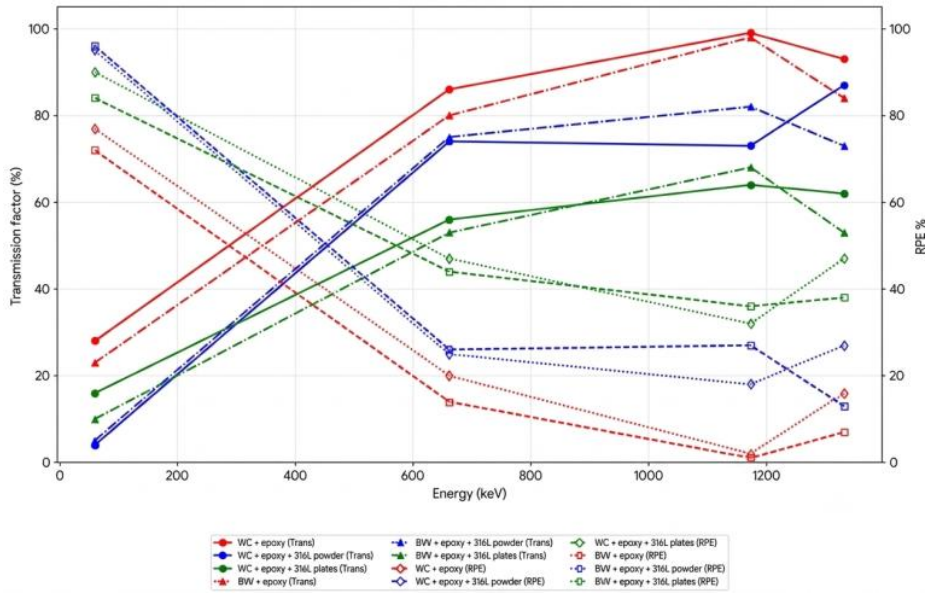

Fig. 6. Variations in the experimental transmission factor (left y-axis, solid/dash-dot lines) and radiation protection efficiency (RPE%, right y-axis, dotted/dashed lines with open markers) as a function of incident gamma-ray energy (0 to 1400 keV).

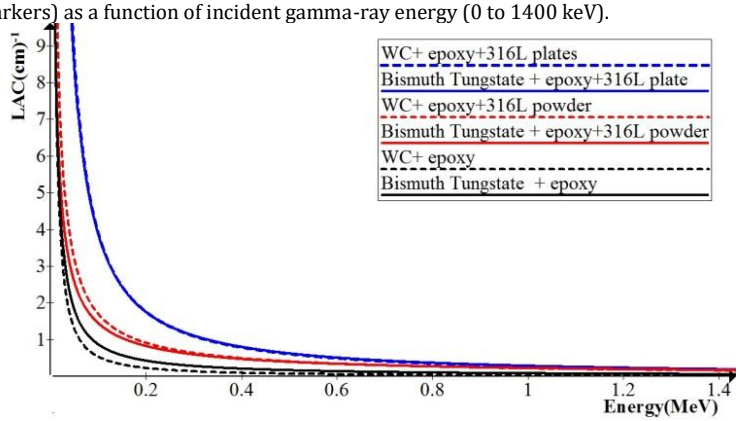

Fig. 7. Linear attenuation coefficient as a function of incident gamma-ray energy for mixtures and multilayers' samples.

4. Conclusions

In this work, Heterogeneous shield transforms from a mere "barrier" into an "integrated shielding system," where each component plays a specific role in achieving comprehensive protection against radiation.

- The competition between the high atomic number of bismuth tungstate components compared to that of WC and the high density of the latter compared to the former led to results that favored tungsten carbide as a better shield than bismuth tungstate.
- Macroscopic structural continuity by using 316L SS plates is more effective than particulate fillers due to continuous interaction paths.
- The method of preparing bismuth tungstate "hydrothermal technique" led to the formation of nanoparticles with micro clusters, and this caused the formation of interstitial spaces that weakened this material as a shield against gamma rays.
- Composite mixtures of epoxy, 316L SS micropowder, and nanoparticles (WC or Bi_2WO_6) provided a triple-action defense: high-Z nanoparticles for radiation absorption, 316L SS for photon scattering via the Compton effect, and hydrogen-rich epoxy for neutron moderation.

Acknowledgements

The authors thank Mustansiriyah University for continuous support.

Funding Statement

This research received no specific grant from any funding agency.

Conflicts of Interest

The authors declare that they have no known competing financial interests or personal relationships that could have appeared to influence the work reported in this paper.

Authors Contribution Statement

The research was conceived by Mustafa and implemented by Haneen.

References

[1] Gilys, L., Griškonis, E., Griškevičius, P. and Adliene, D., 2022. Lead Free Multilayered Polymer Composites for Radiation Shielding. *Polymers, 14*, p.1696.

[2] Al-Saleh, W.M., Almutairi, H.M., Sayyed, M.I. and Elsafi, M., 2023. Multilayer radiation shielding system with advanced composites containing heavy metal oxide nanoparticles: a free-lead solution. *Scientific Reports, 13*, p.18429.

[3] Zolkepli, A.S., Tajudin, S.M., Sabri, A.H.A., Noor, A.F.M. and Aziz, M.Z.A., 2022. Monte carlo simulation of multilayer radiation shielding. *Journal of Nuclear and Related Technology*, *19*, pp.1–7.

[4] Abdul Rahman, R.M., Mustafa, Sh.H., and Kareem K. M., 2026. Fabrication of Gamma Multi Layers Shielding Using Nano Bi, W and Pb Powders. *AIP Conf. Proc*. *3396*, p.060003.

[5] Abdul Rahman, R.M., Mustafa, Sh.H., and Kareem K. M., 2024. Multilayer Electrophoretic Deposition for Gamma Attenuation. *Surface Engineering and Applied Electrochemistry*, *60(6),* pp. 914–921.

[6] Chang, L., Zhang, Y., Liu, T., Fang, J., Luan, W., Yang, X. and Zhang, W., 2015. Preparation and characterization of tungsten/epoxy composites for γ-rays radiation shielding. *Nuclear Instruments and Methods in Physics Research Section B*, *356*, pp.88–93.

[7] Demir, E., Akman, F., Almalki, A.S.A., Kaçal, M.R. and Polat, H., 2022. Green Materials for Radiation Shielding: An Overview. *Emerging Nanomaterials*, pp.299–336.

[8] Soylu, H.M., Yurt Lambrecht, F. and Ersöz, O.A., 2015. Gamma radiation shielding efficiency of a new lead-free composite material. *Journal of Radioanalytical and Nuclear Chemistry*, *305*, pp.529–534.

[9] Giménez, M.A.N. and Lopasso, E.M., 2018. Tungsten carbide compact primary shielding for small medium reactor. *Annals of Nuclear Energy*, *116*, pp.210–223.

[10] Elaouni, A., El Ouardi, M., BaQais, A., Arab, M., Saadi, M. and Ait Ahsaine, H., 2023. Bismuth tungstate Bi_2WO_6: a review on structural, photophysical and photocatalytic properties. *RSC Advances*, *13*, pp.17476–17494.

[11] Yan, Q., Zhang, J., Li, Y., Wu, Y. and Wang, J., 2025. Evaluation of gamma rays shielding properties of bismuth tungstate with different morphologies. *Nuclear Engineering and Technology*, *57*, p.103133.

[12] Hossain, Q.S., Rahman, M.A., Islam, M.S. and Ali, M.A., 2023. A combined first principles and experimental approach to Bi_2WO_6 . *RSC Advances, 13*, pp.36130–36143.

[13] Wu, C., Zhang, L., Shen, J., Zhou, M. and Wu, Q., 2019. Enhanced visible-light-driven photocatalytic properties of acceptor dopant Nb^{+5} modified Bi_2WO_6 by tailoring the morphology from 3D hierarchical microspheres to 2D nanosheets. *Applied Surface Science, 484*, pp.112–123.

[14] DM Naser, SH Lafta, MS Hashim, 2024. Antioxidant activity and cytotoxicity of greigite nanoparticles synthesized by hydrothermal technique. *Biotechnology and Applied Biochemistry*, 71(4), pp.960-973.

[15] Buyuk, B. and Tugrul, A., 2014. Comparison of lead and WC-Co materials against gamma irradiation. *Acta Physica Polonica A*, *125*(2), pp.423-425.

[16] Gavrish, V., Cherkashina N. and Chayka T., 2020. Investigations of the influence of tungsten carbide and tungsten oxide nanopowders on the radiation protection properties of cement matrix-based composite materials, *Journal of Physics: Conference Series*, *1652*, p.012008.

[17] Abualroos, N.J., Idris, M.I., Ibrahim, H., Kamaruzaman, M.I. and Zainon, R., 2024. Physical, mechanical, and microstructural characterisation of tungsten carbide-based polymeric composites for radiation shielding application. *Scientific Reports*, *14*(1), p.1375.

[18] Prabhu, S., Bubbly, S.G. and Gudennavar, S.B., 2022. Preparation and characterization of tungsten carbide/epoxy

composites for γ-ray shielding. *AIP Conference Proceedings*, *2451*, p.020035.

[19] Wang, B., Qin, S., Luo, Y., Han, J. and Zhao, S., 2023. A comparative study between pure bismuth/tungsten and the bismuth tungsten oxide for flexible shielding of gamma/X rays. *Radiation Physics and Chemistry*, *208*, p.110906.